Draft version August 5, 2022
Typeset using LaTeX **twocolumn** style in AASTeX631

Multiple channels for the onset of magnetism in isolated white dwarfs

Stefano Bagnulo [1] and John D. Landstreet [1,2]

[1] *Armagh Observatory & Planetarium*
College Hill
Armagh, BT61 9DG, UK
[2] *University of Western Ontario*
1151 Richmond St. N
London, N6A 3KT, Ontario, Canada

ABSTRACT

The presence of a strong magnetic field is a feature common to a significant fraction of degenerate stars, yet little is understood about field origin and evolution. New observational constraints from volume-limited surveys point to a more complex situation than a single mechanism valid for all stars. We show that in high-mass white dwarfs, which are probably the results of mergers, magnetic fields are extremely common and very strong, and appear immediately in the cooling phase. These fields may have been generated by a dynamo active during the merging. Lower mass white dwarfs, which are often the product of single star evolution, are rarely detectably magnetic at birth, but fields appear very slowly, and very weakly, in about a quarter of them. What we may see is an internal field produced in an earlier evolutionary stage that gradually relaxes to the surface from the interior. The frequency and strength of magnetic fields continue to increase to eventually rival those of highly-massive stars, particularly after the stars cool past the start of core crystallisation, an effect that could be responsible for a dynamo mechanism similar to the one that is active in Earth's interior.

Keywords: Stellar magnetic fields(1610) — white dwarf stars(1799) — spectropolarimetry(1973)

1. INTRODUCTION

Almost all stars with initial masses below about 8 $M_\odot$, whether single or in close binary systems, end their nuclear evolution by collapsing to the white dwarf (WD) state. The basic structure and the cooling history of WDs have been understood for many decades (Chandrasekhar 1931; Mestel 1952). However, the vast literature on these objects indicates that many aspects of the formation, structure and cooling of such stars have turned out to be extremely complicated. One aspect of this complication is the presence of global magnetic fields at the surfaces of some, but not all, WDs. The observed fields range in strength from about 30 kG to several hundred MG (Bagnulo & Landstreet 2021). They have a structure organised at a large scale, often dipole-like, and do not appear to evolve on an observable time scale, although an observed field sometimes varies periodically due to WD rotation.

The origin of magnetic fields in WDs is not well understood, but several ideas have been put forward to explain their presence, for example that the currently visible field is a descendant of a field that was present when the star was in a previous evolutionary stage, or that the observed field is generated by a contemporary dynamo excited in the core of a rotating WD by the convection produced by sinking solids when crystallisation begins (Isern et al. 2017; Ginzburg et al. 2022). Another family of field generation mechanisms suggest that a field is produced by close binary evolution, for example by a dynamo acting during a post common envelope phase (Tout et al. 2008; Briggs et al. 2018), or by a dynamo that is active during the merger of a binary pair of WDs which become a single star (García-Berro et al. 2012).

The only way we know to test these theories is to consider their implications for the population of WDs, and compare predictions with observations. However, observations do not automatically give a clear view of possible correlations between the presence of a magnetic field and other characteristics of the star (such as age or mass), because of the prevalent use of output from low-resolution spectroscopy and of magnitude-limited surveys which strongly skew the sample of known magnetic WDs (MWDs) towards hot stars with field strength in

the range $\sim 2-100$ MG, as will be discussed in Sect. 2. A previous attempt to avoid these biases is represented by the spectropolarimetric survey of the 20 pc volume (Bagnulo & Landstreet 2021), in which more than 20 % of WDs were found to host magnetic fields. An important characteristics of the local 20 pc volume is that MWDs with $M \leq 0.75\,M_{\odot}$ and older than ~ 2 Gyr are quite numerous, more than one out of four WDs, while among 20 WDs younger than 0.5 Gyr, only one is magnetic. The 20 pc volume still includes only a relatively small sample of WDs, none of them belonging to the group of (rare) highly massive WDs. Increasing the volume completely surveyed with spectropolarimetric techniques so as to achieve a significant increase of the survey S/N would require a huge observational effort. It is possible, however, to start the systematic exploration of certain slices of the age-mass space, and obtain a limited yet still unbiased view of the occurrence of the magnetism in, for example, specific age ranges of degenerate stars. Here we report important discoveries from a spectropolarimetric survey of the WDs younger than ~ 600 Myr of the local 40 pc volume.

2. OBSERVATIONAL BIASES IN THE LITERATURE

The first discovery of a magnetic field in a degenerate star was made about fifty years ago via the detection of a signal of broadband circular polarisation, which was ascribed to an effect of dichroism of the continuous opacity caused by the presence of a magnetic field of at least several tens of MG (Kemp et al. 1970). A dozen more WDs were subsequently discovered to be strongly magnetic using the same technique of detection of circular polarisation of the continuum (Landstreet 1992), but since the 1990s, the great majority of MWDs have been discovered via the detection of the Zeeman effect in the spectral lines, either observed with a normal spectrograph sensitive to the light intensity, or via spectropolarimetry, sensitive also to the circular polarisation of the line profiles. A few hundred WDs have been checked for magnetic fields by specifically dedicated spectropolarimetric surveys (e.g. Schmidt & Smith 1995; Putney 1997; Kawka et al. 2007; Kawka & Vennes 2012; Bagnulo & Landstreet 2018, 2021), but the bulk of discoveries of MWDs have been obtained as a by-product of large spectroscopic surveys carried out in a broader astrophysical context, such as the Sloan Digital Sky Survey (SDSS) (Kepler et al. 2013), or of surveys of WDs not specifically aimed at field detection (Liebert et al. 2003; Napiwotzki et al. 2020). Today, we know of more than 600 MWDs (Ferrario et al. 2015), more than half of which were discovered from low-resolution, mostly low S/N SDSS data, which are typically sensitive to field strength between 2 and 100 MG (Kepler et al. 2013). Even high-resolution spectroscopy cannot detect fields weaker than a few tens kG because in that low-field regime, Zeeman splitting is washed out by intrinsic pressure broadening of the spectral lines. At the higher end of field strength (100 MG or more), MWDs may escape detection via spectroscopy because in that regime the magnetic energy becomes comparable to the atomic Coulomb energy, and the position and strength of the components of spectral lines changes to the extent that spectra become difficult to recognise and classify (Wunner et al. 1985). In all WDs that are sufficiently cool to have featureless spectra, the magnetic fields are totally undetectable via spectroscopy (unless their atmospheres are polluted by metal elements). However, due to the dichroism of the continuous opacity (Kemp 1970), starlight is polarised when a strong field is present, hence strongly magnetised WDs may be detected via spectro- or broadband polarimetry even when spectroscopically they would appear featureless or unrecognisable.

Circular spectropolarimetry allows us to measure the longitudinal component of the magnetic field, averaged over the stellar disk, with a sensitivity that in WDs with deep lines may be as good as a few hundred Gauss (if the S/N is sufficiently high), and is the technique of choice to detect stellar magnetic fields. However, because several large systematic spectroscopic surveys are continuously run by large research groups, while spectropolarimetric surveys are much less common, and require much higher S/N than spectroscopy, our knowledge of the magnetism of WDs is very strongly skewed towards MWDs with deep spectral lines and with field strength between 1 and 100 MG.

Another important bias comes from the fact that large surveys are often magnitude-limited. This kind of bias is quantified in Figure 1, which shows the histograms of the age distribution of the sample of all WDs present in the local 40 pc volume, and of the age distribution of a sample of similar size of all WDs with magnitude $G < 15.5$. It clearly appears that young WDs, much brighter than older WDs, are vastly over-represented in magnitude limited surveys. We find that 77 % of the WDs of the magnitude-limited sample are younger than 0.5 Gyr, while they represent only 11 % of the volume-limited sample. Stars older than 3.5 Gyr make up 40 % of the WDs within 40 pc from the Sun, while they represent only 1.5 % of the WDs brighter than $G = 15.5$. Furthermore, due to the way spectral features change with temperature (hence cooling age), magnetic fields are detected with a higher sensitivity in younger WDs than in older WDs. As a result, collecting spectroscopic

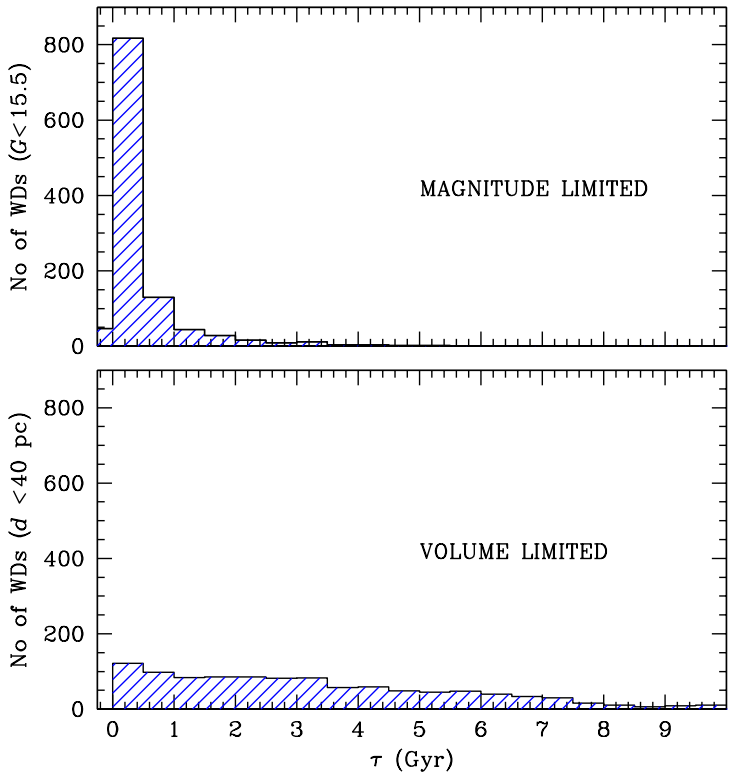

Figure 1. Age distribution of a magnitude limited sample (top panel) and a volume limited sample (bottom panel) of similar size ($\sim$ 1000 WDs). Cooling age was estimated using the mass and temperature from the most recent WD catalogue of Gentile Fusillo et al. (2021) assuming that all stars are H-rich, and interpolating the age from the table of the Montreal group (Bédard et al. 2020) using the results for thick hydrogen layer models.

measurements from magnitude-limited surveys may reveal in which kind of star field detection techniques are most effective, rather than the kinds of star in which fields are more frequently present. The ratio of known MWDs of a certain age to the total number of known MWDs may not reflect at all the way in which the frequency of the occurrence of magnetic fields varies with age.

3. NEW OBSERVATIONS

Gaia photometry and parallaxes allow the identification of 1077 WDs (with a probability of WD nature $p > 0.75$) in the volume of space within 40 pc from the Sun (Gentile Fusillo et al. 2021), and provide estimates for their temperatures and masses. We have then estimated the ages of the stars of this sample by interpolating the Montreal WD evolutionary sequence tables by Bédard et al. (2020), and finally identified about 145 WDs younger than 600 Myr, including about 20 WDs that are within the local 20 pc volume and that were already discussed in a previous survey (Bagnulo & Landstreet 2021). A literature search showed that 11 of the young WDs within 40 pc from the Sun had already been found to be magnetic by previous work, and that another 64 had been observed in spectropolarimetric mode and found non-magnetic (details are given in App. B).

For our new observations we have used the FOcal Reducer and low dispersion Spectrograph (FORS2) instrument of the ESO Very Large Telescope (Appenzeller et al. 1998), the Echelle SpectroPolarimetric Device for the Observation of Stars (ESPaDOnS) instrument of the Canada-France-Hawaii telescope (Donati et al. 2006), and the Intermediate-dispersion Spectrograph and Imaging System (ISIS) on the William Herschel Telescope. With these instruments we obtained 107 new spectropolarimetric observations of 85 young WDs between 20 and 40 pc from the Sun. Among them, 58 had never been observed in polarimetric mode before; for the majority of the remaining 27 stars, we improved the sensitivity of the measurements typically by at least a factor of 5. Only a dozen stars, mostly with ages in the range 0.5–0.6 Gyr, were left unchecked for magnetic field. Observing strategy, data reduction, and results for individual stars are described in detail in App. A, where we report the discovery of a strong magnetic field in the high-mass star WD 1008−242 = UCAC4 328-061594, a

confirmed detection of a weak field in the high-mass WD 0232+525 (Bagnulo & Landstreet 2021), a probable but to be confirmed detection of a weak field in the average mass star WD 1704+481.1, and no field detection in any of the remaining 82 young WDs.

4. RESULTS

Our new spectropolarimetric observations, combined with previous data collected in volume-limited samples, show that $\sim$ 10 % of WDs younger than 0.6 Gyr and within 40 pc from the Sun are magnetic. Remarkably, the mass distribution of the young MWDs is highly skewed towards the highest values. Although $\sim$ 0.6 % of the WDs of the 40 pc volume younger than 600 Myr have $M \geq 1.1\,M_\odot$, more than half of the young MWDs of the same volume are in that mass range, and ten out of the 12 (or 13) young MWDs have $M \geq 0.75\,M_\odot$. The average mass of the MWDs younger than 0.6 Gyr is $0.98\,M_\odot$ (with a scattering of $\sim 0.26\,M_\odot$), while the average mass of the nMWDs in the same age range is $0.62 \pm 0.14\,M_\odot$. This is in stark contrast to what is observed in stars with cooling age $\geq$ 2 Gyr, among which the average mass of MWDs is practically indistinguishable than that of nMWDs ($0.65 \pm 0.12\,M_\odot$ and $0.62 \pm 0.13\,M_\odot$ for the MWDs and nMWDs, respectively). Previous literature has repeatedly highlighted that the average mass of MWDs is higher than the average mass of nMWDs (Liebert 1988; Kepler et al. 2013; McCleery et al. 2020). The new results provide a clearer view: young MWDs are generally highly massive, while magnetic fields appear in lower mass WDs only when they are older. Therefore, the average mass of younger MWDs is higher than the average mass of older MWD.

Figure 2 shows the position of all WDs of the 20 pc volume plus all observed young WDs of the local 40 pc volume (for a total of 264 stars), in a diagram of mass versus cooling age τ. Notice that although different volumes are combined, each half of the diagram refers to a volume-limited sample.

The picture that we infer is that, among the WDs younger than 0.6 Gyr, almost all those with $M > 1.1\,M_\odot$ are magnetic ($\sim$ 85 %), and almost all those with $M \leq 0.75\,M_\odot$ are non-magnetic ($\lesssim$ 2.5 %). Furthermore, the field strengths of all high-mass MWDs except one are very high (ranging from $\sim$ 3 to 300 MG), while the fields of the few lower mass MWDs are much weaker in strength, mostly of order of tens of kG, and stay weak for a long time: among lower mass WDs, the youngest one that shows a MG field is almost 2 Gyr old. In the intermediate mass regime between 0.75 and $0.95 M_\odot$, three out of 20 young WDs are magnetic. Two of these MWDs have very weak fields, one has a very strong field. These stars may belong to an overlap region between lower (normal) mass, mostly nMWDs, and high-mass, mostly magnetic WDs. The star with the strongest field (700 MG) has $M = 0.9\,M_\odot$ and may well belong to the category of high-mass, high-field strength WDs. The mass range 0.95 to $1.10\,M_\odot$ is not probed by our observations in young stars, and clearly more data are needed to better sample the transition mass region, as current data leave a certain degree of arbitrariness in the definition of the mass threshold values.

5. INTERPRETATION

The fundamental discovery emerging from the new data is the clear identification of two populations distinguished by very different typical masses, that exhibit entirely different evolutions of magnetism. Among the most massive WDs, which represent a tiny minority of all WDs, large magnetic fields are frequent and emerge to the stellar surface immediately or shortly (within hundreds of Myr) after the start of the cooling phase, with typical strengths that are among the largest observed in WDs, often above 100 MG. Among the young WDs with masses below $\sim 0.75 M_\odot$, values that are perfectly typical of the large majority of WDs, magnetic fields are extremely rare, down to field detection limits of a few kG, and the few fields found are among the weakest ones found in degenerate stars. The strength and frequency of the surface fields of lower mass WDs grow slowly with time: among lower mass WDs, the youngest one that shows a MG field is almost 2 Gyr old; then 11 out of 64 WDs older than 3 Gyr with $M \leq 0.75\,M_\odot$ have a magnetic field with strength in the same range as that typical of high-mass, young strongly magnetic WDs. Old, weakly magnetic WDs are also present, and may well be more numerous than found, because weak fields are difficult to detect in cool WDs, unless strong metal lines are present. It is remarkable how well our new, statistically strong, and evolutionarily clear picture agrees with the trends extracted from very heterogeneous data by Valyavin & Fabrika (1999), who had suggested already the existence of two populations of MWDs similar to those found in this survey.

Mass is normally a conserved quantity as a single WD cools, so the two groups maintain their identities as they cool. The evolution of the frequency of the occurrence of MWDs in these two groups of stars with time is visualised in the left panels of Fig. 3. Now we consider how these two very different evolution paths may have arisen.

The most massive MWDs are often supposed to have been formed by an evolution pathway involving the merger of two WDs created during the evolution of a

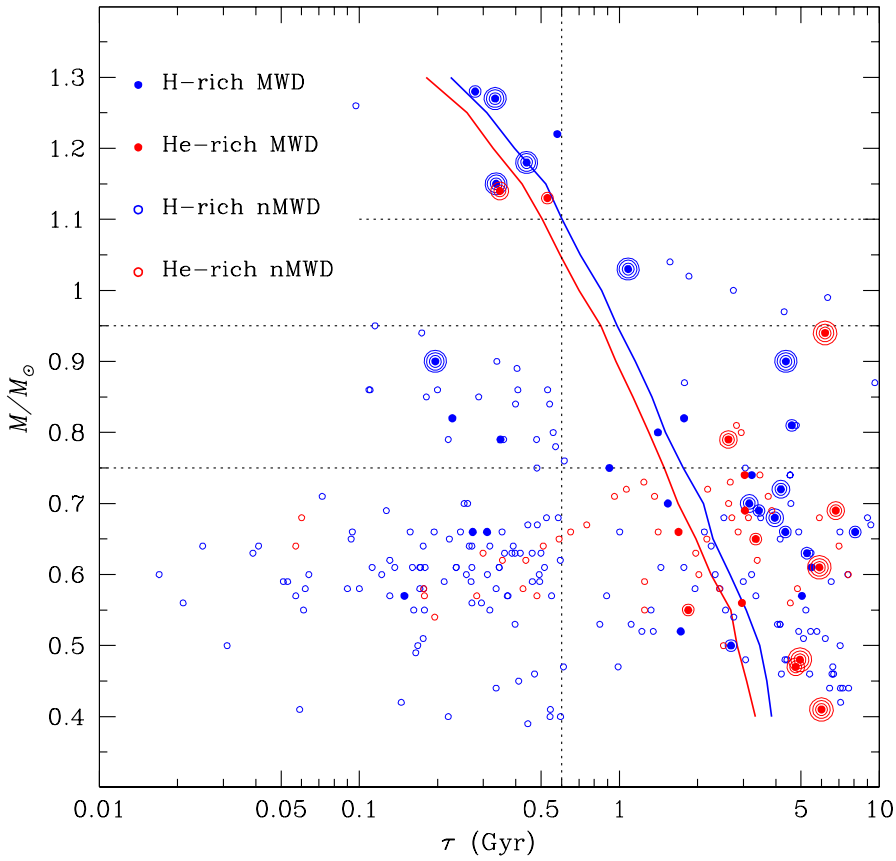

Figure 2. Age-mass diagram using data obtained for all WDs of the local 20 pc volume and most of the WDs younger than 0.6 Gyr up to 40 pc from the Sun. Stellar parameters are obtained as explained in App. B and given in Table 2. Filled dots identify MWDs with fields below 1 MG; filled dots surrounded by one circle represent MWDs with field strength between 1 and 10 MG, filled dots surrounded by two circles represent MWDs with field strength between 10 and 100 MG, and filled dots surrounded by three circles represent MWDs with field strength $\geq$ 100 MG. Solid curves represent the onset of crystallisation; the red line refers to thin hydrogen layer models, and the blue line to thick hydrogen layers models as provided by theoretical computations (Bédard et al. 2020). The vertical dotted line marks the age limit of the 40 pc survey; the horizontal dotted lines mark the mass boundaries discussed in the text.

close binary system (Ferrario et al. 1997; Dobbie et al. 2012). It has been argued that such a merger could lead to the generation of a very strong magnetic field, and it seems plausible that such a field would almost immediately be present at the WD surface (García-Berro et al. 2012). Furthermore, this merger event would generally be expected to leave a strong footprint in the form of a very rapid rotation of the resulting star, a feature that is found in several massive MWDs (Barstow et al. 1995; Schmidt & Norsworthy 1991; Pshirkov et al. 2020). An alternative formation route for the most massive MWDs might be through single-star evolution from the most massive main sequence stars that collapse to become WDs at the end of their lives. The detection of strong magnetic fields in three massive WDs belonging to young clusters has led to the claim that intermediate-mass main sequence stars (with $M \geq 5\,M_{\odot}$) have a high probability of producing relatively massive MWDs (Richer et al. 2019; Caiazzo et al. 2020). However, this hypothesis does not find support in the larger number of spectroscopically observed WDs of $M \approx 1\,M_{\odot}$ in other young clusters for which no magnetic fields are reported (Cummings et al. 2018), and which are also very probably produced by single star evolution. In addition, it is unclear why such a mechanism would frequently or rapidly generate a magnetic field in WDs descended from stars with main sequence mass higher than a certain value, but would cease to be effective in WDs descended from less massive progenitors. Therefore we provisionally adopt the binary merger hypothesis for the formation of the most massive and strongly magnetic WDs of our sample.

We next consider the possible origin of the rare weak fields in the main sample of the youngest normal-mass WDs, in which magnetism is so rare and so weak. In such stars, there does not seem to be any proposed dy-

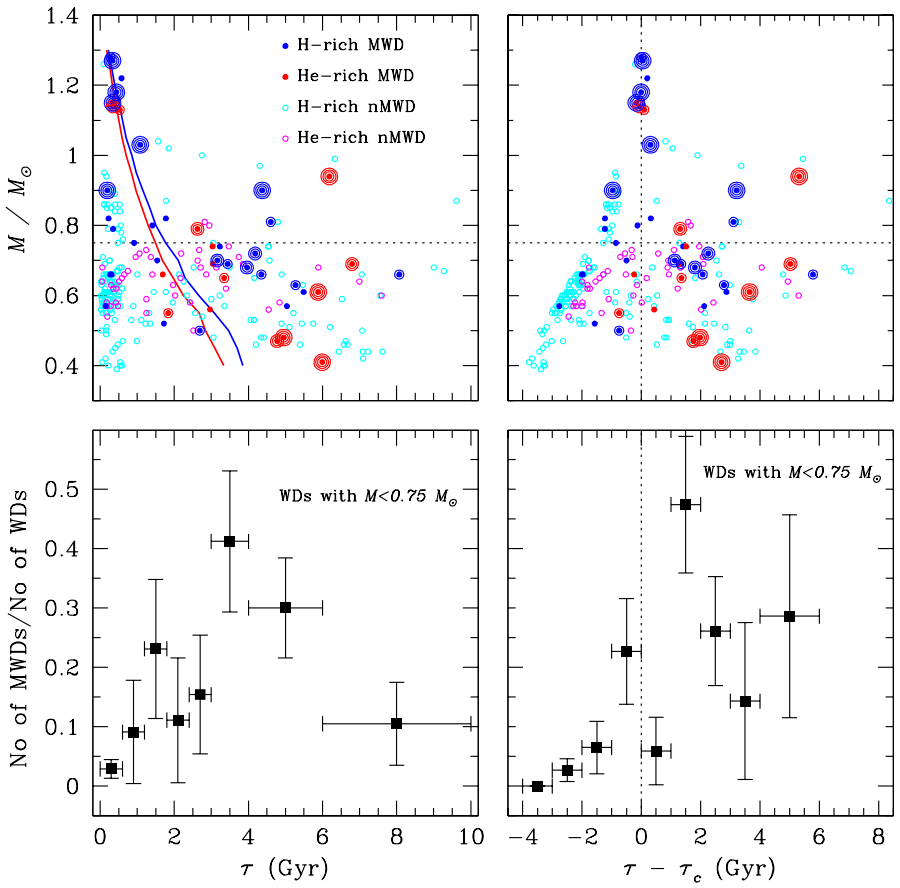

Figure 3. *Top panels:* Magnetic and non magnetic WDs in a age-mass diagram, with age expressed in a linear scale. The meaning of the symbols is the same as in Fig. 2. *Bottom panels:* the observed distribution of the ratio between MWDs and total number of WDs with $M \leq 0.75\,M_{\odot}$. The left panels refer to the cooling age, while in the right panels the age is counted from the onset of crystallisation, which varies from star to star according to mass.

namo mechanism acting in the interior of the WDs, at least until they cool enough for core crystallisation to begin. We deduce that the fields that begin to appear very weakly in young WDs, and appear more and more strongly as time goes on during the first 2 or 3 Gyr, are probably fields left from earlier stages of evolution in the interior of newly formed normal-mass WDs. If this is the case, it appears that we may be witnessing the relaxation of a pre-existing field buried in the interior of a WD during its evolution as a main sequence or giant star. The relaxation time should probably be of the order of the global field decay timescale, which is estimated of the order of 2 Gyr (Fontaine et al. 1973). This time scale would roughly agree with the time scale over which we find fields emerging to the surfaces of MWDs. The way in which such relaxation might occur has been studied using numerical MHD simulations by Braithwaite & Spruit (2004), who have shown that an arbitrary initially unstable, complex field relaxes rather rapidly to a mixture of an interior toroidal field and a global poloidal (dipolar) field, which is stable. The dipolar field, which is what appears at the surface, continues to increase in strength even though the global interior field is decreasing due to resistivity.

If this picture is correct, we have not solved the puzzle of the origin of the fields observed in some normal-mass WDs, but merely displaced the origin to an earlier or later mechanism. One possible field origin may be the magnetic fields apparently detected by using asteroseismology tools on Kepler photometry (Stello et al. 2016) in the cores of some red giants. Another possible source could be a dynamo operating in a shell undergoing fusion (Kissin & Thompson 2015). In contrast, the nearly total lack of fields in the youngest normal-mass WDs may pose a serious problem for one of the oldest theories of WD field origins, the retention (freezing) and amplification of the magnetic flux observed in the atmospheres of the (chemically peculiar) Ap and Bp main sequence stars (Woltjer 1964; Landstreet 1967; Angel et al. 1981). It is not at all clear why the magnetic sur-

face flux observed on the main sequence should retreat into the stellar interior later in evolution, only to very slowly leak back out to the stellar surface long after the formation of the WD.

It has been remarked that cool WDs that exhibit metal lines in their spectra are more frequently magnetic than any other class of WDs (Hollands et al. 2017; Kawka et al. 2019; Bagnulo & Landstreet 2019; Kawka et al. 2021), and this has been seen as a hint that the presence of a magnetic field is an effect of accretion from a debris disk (Farihi et al. 2011; Kawka & Vennes 2014). However, this correlation can be simply interpreted as the combination of the increase of the frequency of magnetic fields with cooling age and the fact that the presence of metal lines in cool stars enormously increases the sensitivity of the magnetic field measurements (Hollands et al. 2017; Bagnulo & Landstreet 2020). The latter interpretation seems supported by the fact that among older WDs of the 20 pc volume, the frequency of the occurrence of the magnetic field is similar in WDs that exhibit metal lines in their spectra, and in WDs that do not show metal lines (Bagnulo & Landstreet 2021).

In recent years there has been much discussion about whether the magnetic field of WDs could be generated by a dynamo mechanism similar to the one that produces the fields of the Earth and of M dwarfs. This dynamo would be powered by the core convection that occurs when the WD degenerate core begins to crystallise in the presence of stellar rotation. Initial estimates suggested that this mechanism would require quite rapid rotation, and would at most be able to produce fields of order 1 MG (Isern et al. 2017). Since the original formulation of the theory, two significant modifications have been proposed that extend considerably its potential importance. First, that the field generated by this dynamo is orders of magnitude stronger than that originally estimated, in such a way to justify the observed range of field strengths (Schreiber et al. 2021). Secondly, that the convection is much slower than originally estimated (Ginzburg et al. 2022). These modifications lead to a dynamo that requires much less rapid rotation and one that readily produces fields of the order of 100 MG, suggesting more strongly that crystallisation might play an important part in producing the fields in about 20% of normal-mass WDs older than about $\sim 2-3$ Gyr.

The boundary of physical conditions under which a crystallisation-driven dynamo could begin to operate is shown in Fig. 2 and in the top panels of Fig. 3 with two close oblique lines which refer, respectively, to WDs with almost no H envelope, and WDs with thick H envelopes. These two lines provide an estimate of the uncertainty of the age at which crystallisation starts for any particular WD. It is clear that some fields arise well before crossing the crystallisation line. Therefore this dynamo cannot be the only source of magnetic fields in lower mass WDs. However, the frequency of MWDs appears to increase after the crystallisation line. This is explored more quantitatively in the right-hand panels of Fig. 3 in which the abscissa coordinate is cooling time measured before and after the onset of crystallisation for each mass. This figure shows a steady rise in the magnetic WD fraction as a function of this time, both before and after the onset of crystallisation. The MWD frequency among normal-mass WDs does not change as the crystallisation boundary is crossed, but approximately doubles as another Gyr elapses, before falling off, perhaps because of ohmic decay, or perhaps simply because in older stars, which are generally faint and featureless, only fields stronger than a few MG may be detected. It appears that the crystallisation dynamo may well contribute significantly to the normal-mass, old, cool MWD cohort. To better understand its role, future observations should target WDs just before and after the beginning of the crystallisation phase.

Based on observations obtained at with the FORS2 instrument at the ESO Telescopes at the La Silla Paranal Observatory under program ID 109.235.Q001, 108.2206.001, 108.2206.002, and 0101.D-0103(C); with ESPaDOnS on the Canada-France-Hawaii Telescope (CFHT) (operated by the National Research Council (NRC) of Canada, the Institut National des Sciences de l'Univers of the Centre National de la Recherche Scientifique (CNRS) of France, and the University of Hawaii), under programmes 15BC05, 16AC05, 16BC01, 17AC01, 18AC06, 18BC02, 21BC002 and 22AC023; and with the ISIS instrument at the William Herschel Telescope (operated on the island of La Palma by the Isaac Newton Group), under programmes P15 in 18B, P10 in 19A and P8 in 19B. The observations at the CFHT were performed with care and respect from the summit of Maunakea which is a significant cultural and historic site. All raw data and calibrations of FORS2, ISIS and ESPaDOnS data are available at the observatory archives: ESO archive at `https://archive.eso.org`; Astronomical Data Centre at `http://casu.ast.cam.ac.uk/casuadc/`; and the Canadian Astronomical Data Centre at `https://www.cadc-ccda.hia-iha.nrc-cnrc.gc.ca/en/`.
This work has made use of data from the European Space Agency (ESA) mission *Gaia* (https://www.cosmos.esa.int/gaia), processed by the *Gaia* Data Processing and Analysis Consortium (DPAC, https://www.cosmos.esa.int/web/gaia/dpac/consortium). Funding for the DPAC has been provided by national institutions, in particular the institutions participating in the *Gaia* Multilateral Agreement. JDL acknowledges the financial support of the Natural Sciences and Engineering Research Council of Canada (NSERC), funding reference number 6377-2016.

REFERENCES

Angel, J. R. P., Borra, E. F., & Landstreet, J. D. 1981, ApJS, 45, 457, doi: 10.1086/190720

Appenzeller, I., Fricke, K., Fürtig, W., et al. 1998, The Messenger, 94, 1

Aznar Cuadrado, R., Jordan, S., Napiwotzki, R., et al. 2004, A&A, 423, 1081, doi: 10.1051/0004-6361:20040355

Bagnulo, S., Landolfi, M., Landstreet, J. D., et al. 2009, PASP, 121, 993, doi: 10.1086/605654

Bagnulo, S., & Landstreet, J. D. 2018, A&A, 618, A113, doi: 10.1051/0004-6361/201833235

—. 2019, A&A, 630, A65, doi: 10.1051/0004-6361/201936068

—. 2020, A&A, 643, A134, doi: 10.1051/0004-6361/202038565

—. 2021, MNRAS, 507, 5902, doi: 10.1093/mnras/stab2046

Bagnulo, S., Szeifert, T., Wade, G. A., Landstreet, J. D., & Mathys, G. 2002, A&A, 389, 191, doi: 10.1051/0004-6361:20020606

Barstow, M. A., Jordan, S., O'Donoghue, D., et al. 1995, MNRAS, 277, 971, doi: 10.1093/mnras/277.3.971

Bédard, A., Bergeron, P., Brassard, P., & Fontaine, G. 2020, ApJ, 901, 93, doi: 10.3847/1538-4357/abafbe

Braithwaite, J., & Spruit, H. C. 2004, Nature, 431, 819, doi: 10.1038/nature02934

Briggs, G. P., Ferrario, L., Tout, C. A., & Wickramasinghe, D. T. 2018, MNRAS, 478, 899, doi: 10.1093/mnras/sty1150

Caiazzo, I., Heyl, J., Richer, H., et al. 2020, ApJL, 901, L14, doi: 10.3847/2041-8213/abb5f7

Chandrasekhar, S. 1931, ApJ, 74, 81, doi: 10.1086/143324

Cummings, J. D., Kalirai, J. S., Tremblay, P. E., Ramirez-Ruiz, E., & Choi, J. 2018, ApJ, 866, 21, doi: 10.3847/1538-4357/aadfd6

Dobbie, P. D., Baxter, R., Külebi, B., et al. 2012, MNRAS, 421, 202, doi: 10.1111/j.1365-2966.2012.20291.x

Donati, J.-F., Howarth, I. D., Bouret, J.-C., et al. 2006, MNRAS, 365, L6, doi: 10.1111/j.1745-3933.2005.00115.x

Donati, J. F., Morin, J., Petit, P., et al. 2008, MNRAS, 390, 545, doi: 10.1111/j.1365-2966.2008.13799.x

Dufour, P., Blouin, S., Coutu, S., et al. 2017, in Astronomical Society of the Pacific Conference Series, Vol. 509, 20th European White Dwarf Workshop, ed. P. E. Tremblay, B. Gaensicke, & T. Marsh, 3. https://arxiv.org/abs/1610.00986

Farihi, J., Dufour, P., Napiwotzki, R., & Koester, D. 2011, MNRAS, 413, 2559, doi: 10.1111/j.1365-2966.2011.18325.x

Ferrario, L., de Martino, D., & Gänsicke, B. T. 2015, SSRv, 191, 111, doi: 10.1007/s11214-015-0152-0

Ferrario, L., Vennes, S., Wickramasinghe, D. T., Bailey, J. A., & Christian, D. J. 1997, MNRAS, 292, 205, doi: 10.1093/mnras/292.2.205

Fontaine, G., Thomas, J. H., & van Horn, H. M. 1973, ApJ, 184, 911, doi: 10.1086/152381

García-Berro, E., Lorén-Aguilar, P., Aznar-Siguán, G., et al. 2012, ApJ, 749, 25, doi: 10.1088/0004-637X/749/1/25

Gentile Fusillo, N. P., Tremblay, P. E., Cukanovaite, E., et al. 2021, MNRAS, 508, 3877, doi: 10.1093/mnras/stab2672

Ginzburg, S., Fuller, J., & Kawka, A. 2022, arXiv e-prints, arXiv:2202.12902. https://arxiv.org/abs/2202.12902

Hollands, M. A., Koester, D., Alekseev, V., Herbert, E. L., & Gänsicke, B. T. 2017, MNRAS, 467, 4970, doi: 10.1093/mnras/stx250

Isern, J., García-Berro, E., Külebi, B., & Lorén-Aguilar, P. 2017, ApJL, 836, L28, doi: 10.3847/2041-8213/aa5eae

Jordan, S., Aznar Cuadrado, R., Napiwotzki, R., Schmid, H. M., & Solanki, S. K. 2007, A&A, 462, 1097, doi: 10.1051/0004-6361:20066163

Kawka, A., & Vennes, S. 2012, MNRAS, 425, 1394, doi: 10.1111/j.1365-2966.2012.21574.x

—. 2014, MNRAS, 439, L90, doi: 10.1093/mnrasl/slu004

Kawka, A., Vennes, S., Allard, N. F., Leininger, T., & Gadéa, F. X. 2021, MNRAS, 500, 2732, doi: 10.1093/mnras/staa3421

Kawka, A., Vennes, S., Ferrario, L., & Paunzen, E. 2019, MNRAS, 482, 5201, doi: 10.1093/mnras/sty3048

Kawka, A., Vennes, S., Schmidt, G. D., Wickramasinghe, D. T., & Koch, R. 2007, ApJ, 654, 499, doi: 10.1086/509072

Kemp, J. C. 1970, ApJ, 162, 169, doi: 10.1086/150643

Kemp, J. C., Swedlund, J. B., Landstreet, J. D., & Angel, J. R. P. 1970, ApJL, 161, L77, doi: 10.1086/180574

Kepler, S. O., Pelisoli, I., Jordan, S., et al. 2013, MNRAS, 429, 2934, doi: 10.1093/mnras/sts522

Kissin, Y., & Thompson, C. 2015, ApJ, 809, 108, doi: 10.1088/0004-637X/809/2/108

Koester, D., Dreizler, S., Weidemann, V., & Allard, N. F. 1998, A&A, 338, 612

Landstreet, J. D. 1967, Physical Review, 153, 1372, doi: 10.1103/PhysRev.153.1372

—. 1992, A&A Rv, 4, 35, doi: 10.1007/BF00873569

Landstreet, J. D., & Bagnulo, S. 2019a, A&A, 623, A46, doi: 10.1051/0004-6361/201834638

—. 2019b, A&A, 628, A1, doi: 10.1051/0004-6361/201936009

—. 2020, A&A, 634, L10, doi: 10.1051/0004-6361/201937301
Landstreet, J. D., Bagnulo, S., Valyavin, G., & Valeev, A. F. 2017, A&A, 607, A92, doi: 10.1051/0004-6361/201731432
Landstreet, J. D., Bagnulo, S., Valyavin, G. G., et al. 2012, A&A, 545, A30, doi: 10.1051/0004-6361/201219829
—. 2015, A&A, 580, A120, doi: 10.1051/0004-6361/201526434
Liebert, J. 1988, PASP, 100, 1302, doi: 10.1086/132322
Liebert, J., Angel, J. R. P., Stockman, H. S., Spinrad, H., & Beaver, E. A. 1977, ApJ, 214, 457, doi: 10.1086/155271
Liebert, J., Bergeron, P., & Holberg, J. B. 2003, AJ, 125, 348, doi: 10.1086/345573
Liebert, J., Bergeron, P., Schmidt, G. D., & Saffer, R. A. 1993, ApJ, 418, 426, doi: 10.1086/173403
McCleery, J., Tremblay, P.-E., Gentile Fusillo, N. P., et al. 2020, MNRAS, 499, 1890, doi: 10.1093/mnras/staa2030
McCook, G. P., & Sion, E. M. 1977, A Catalogue of spectroscopically identified white dwarfs
—. 1999, ApJS, 121, 1, doi: 10.1086/313186
Mestel, L. 1952, MNRAS, 112, 583, doi: 10.1093/mnras/112.6.583
Napiwotzki, R., Karl, C. A., Lisker, T., et al. 2020, A&A, 638, A131, doi: 10.1051/0004-6361/201629648
Pshirkov, M. S., Dodin, A. V., Belinski, A. A., et al. 2020, MNRAS, 499, L21, doi: 10.1093/mnrasl/slaa149
Putney, A. 1997, ApJS, 112, 527, doi: 10.1086/313037
Richer, H. B., Kerr, R., Heyl, J., et al. 2019, ApJ, 880, 75, doi: 10.3847/1538-4357/ab2874
Schmidt, G. D., Elston, R., & Lupie, O. L. 1992, AJ, 104, 1563, doi: 10.1086/116341
Schmidt, G. D., & Norsworthy, J. E. 1991, ApJ, 366, 270, doi: 10.1086/169559
Schmidt, G. D., & Smith, P. S. 1995, ApJ, 448, 305, doi: 10.1086/175962
Schreiber, M. R., Belloni, D., Gänsicke, B. T., Parsons, S. G., & Zorotovic, M. 2021, Nature Astronomy, doi: 10.1038/s41550-021-01346-8
Stello, D., Cantiello, M., Fuller, J., et al. 2016, Nature, 529, 364, doi: 10.1038/nature16171
Swedlund, J. B., Wolstencroft, R. D., Michalsky, Jr., J. J., & Kemp, J. C. 1974, ApJL, 187, L121, doi: 10.1086/181412
Tout, C. A., Wickramasinghe, D. T., Liebert, J., Ferrario, L., & Pringle, J. E. 2008, MNRAS, 387, 897, doi: 10.1111/j.1365-2966.2008.13291.x
Valyavin, G., & Fabrika, S. 1999, in Astronomical Society of the Pacific Conference Series, Vol. 169, 11th European Workshop on White Dwarfs, ed. S. E. Solheim & E. G. Meistas, 206
Woltjer, L. 1964, Nature, 201, 803, doi: 10.1038/201803a0
Wunner, G., Roesner, W., Herold, H., & Ruder, H. 1985, A&A, 149, 102

APPENDIX

A. NEW OBSERVATIONS

All our new observations target WDs within 40 pc from the Sun and younger than 0.6 Gyr, identified as explained in App. B. Observing strategy and data reduction are described in detail in numerous previous papers (Bagnulo & Landstreet 2018; Landstreet et al. 2015, 2017), and so are the methods used to measure the longitudinal field from polarised spectral lines (Landstreet et al. 2017; Bagnulo & Landstreet 2018; Landstreet & Bagnulo 2019a). Briefly, the beam-swapping technique is used to minimise the impact of instrumental polarisation (Bagnulo et al. 2009), typically taking four exposures with the retarder waveplate at position angles $\alpha = -45°$, $+45°$, $+45°$, $-45°$. For data obtained with ISIS and FORS2, bias-subtraction, background subtraction, flux extraction and wavelength calibration were performed using standard IRAF routines, while the reduced Stokes V/I profiles were obtained with simple Fortran routines by combining the various beams according to

$$\frac{V}{I} = \frac{1}{2}\left\{ \left(\frac{f_\parallel - f_\perp}{f_\parallel + f_\perp}\right)_{\alpha=-45°} - \left(\frac{f_\parallel - f_\perp}{f_\parallel + f_\perp}\right)_{\alpha=+45°} \right\}, \tag{A1}$$

where $f_\parallel$ and $f_\perp$ are the flux measured in the parallel and perpendicular beam of the beam splitting device (a Wollaston prism in FORS2 and a Savart plate for ISIS), respectively. ESPaDOnS data were reduced by the pipeline LibreEsprit (Donati et al. 2008). The uncertainty of the V/I profile in a spectral bin is approximately given by the inverse of the signal-to-noise ratio accumulated in that spectral bin adding up the fluxes measured in both beams at all positions of the retarder waveplate (Bagnulo et al. 2009). Field measurements were then obtained by minimising the expression:

$$\chi^2 = \sum_i \frac{(y_i - \langle B_z \rangle\, x_i - b)^2}{\sigma_i^2}\,, \tag{A2}$$

where, for each spectral point i, $y_i = V(\lambda_i)/I(\lambda_i)$, $x_i = -g_{\rm eff} C_z \lambda_i^2\, (1/I_i \times {\rm d}I/{\rm d}\lambda)_i$, and b is a constant introduced to account for possible spurious polarisation in the continuum, $g_{\rm eff}$ is the effective landé factor, and

$$C_z = \frac{e}{4\pi m_{\rm e} c^2} \qquad (\simeq 4.67 \times 10^{-13}\ {\rm \AA}^{-1}\ {\rm G}^{-1}) \tag{A3}$$

where e is the electron charge, $m_{\rm e}$ the electron mass, and c the speed of light. The alignment of the polarimetric optics was checked by measuring the magnetic field of well known magnetic stars, WD 1900+705 in case of ISIS, and the Ap star HD 94660 in case of FORS2, which both display a nearly constant longitudinal field. For example, we know that HD 94660 shows a longitudinal field, measured from the H Balmer lines, of ~ -2.0 kG (Bagnulo et al. 2002). We observed this star on night 2021-12-28 and measured $\langle B_z \rangle = -2.09 \pm 0.01$ kG. The spectral analysis of HD 94660 is illustrated in Fig. 4, while an example with a WD is shown in Fig. 5. We note that in both cases, no obvious Zeeman effect is visible in the intensity profiles of the spectral lines, but the presence of a magnetic field is revealed by the analysis of their circular polarisation.

The observing log is given in Table 1. We confirm the discovery of a magnetic field (with ISIS and ESPaDOnS) in WD 0232+525, a discovery that was already anticipated in a previous work (Bagnulo & Landstreet 2021), and of a signal of circular polarisation in the continuum of WD 1008−242 of order 1 % with FORS2 (see Fig. 6), that we interpret with the presence of a ~ 150 MG magnetic field (based on some semi-empirical rules that associate the fraction of circular polarisation to the magnetic field strength Bagnulo & Landstreet 2020). Detection of a weak field was obtained with ESPaDOnS on star WD 1704+481.1, but this detection definitely needs to be checked again with future observations. No field was found in any of the remaining observed stars (see Table 1).

B. DATA USED IN THIS WORK

All data used in this paper are shown in Table 2 and include two volume limited samples of WDs that have been checked for the presence of a magnetic field, which means that either a field has been firmly detected either via spectroscopic or spectropolarimetric techniques, or highly-sensitive field measurements have been performed by spectropolarimetric techniques, resulting into non-detection. The first sample includes virtually all WDs within 20 pc

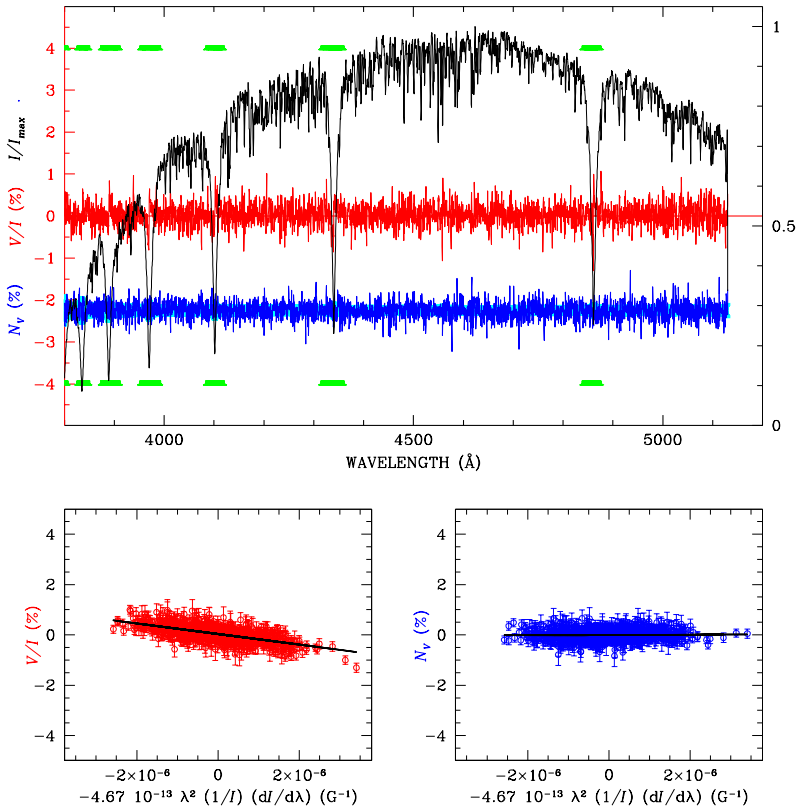

Figure 4. In the upper panel, the black solid line shows the intensity profile of the magnetic Ap star HD 94660, normalised to its maximum (its scale is given in the right axis). The shape of the intensity is due to the star's spectral energy distribution convolved with the transmission function of the atmosphere + telescope optics + instrument. The red solid line shows the V/I profile (in % units, the scale is on the left-hand axis) and the blue solid line is the null profile offset by $-2.25\,\%$ for display purpose. The null profile is the difference between the V/I profiles measured from two different pairs of exposures, and represents an experimental estimate of the noise. Photon-noise error bars are also shown centred around $-2.25\,\%$ and appear as a light blue background. Spectral regions highlighted by green bars have been used to determine the $\langle B_z \rangle$ value from H Balmer lines. The two bottom panels show the best-fit obtained by minimising the expression of Eq. (A2) using the V/I profiles (left panel) and the null profiles (right panel). Data were obtained with FORS2 using grism 1200B.

from the Sun, already analysed by Bagnulo & Landstreet (2021). The second sample, which was newly obtained for this work, is a nearly complete extension to the local 40 pc volume of the population of WDs younger than 0.6 Gyr, the list of which was identified with the help of the catalogue by Gentile Fusillo et al. (2021). All together, Table 2 includes $\simeq 99\,\%$ all of WDs of the local 20 pc volume and $\simeq 90\,\%$ of WDs younger than 0.6 Gyr within 40 pc from the Sun.

All stellar ages (col. 8) were estimated by us using the online cooling tables of the Montreal group (Bédard et al. 2020), and a two-dimensional logarithmic interpolation on the effective temperature (given in col. 6) and mass (given in col. 7) deduced from Gaia photometry by Gentile Fusillo et al. (2021). We used thick hydrogen layer models for H-rich atmospheres, thin hydrogen layer models for He-rich atmospheres – the chemical composition of the atmosphere (col. 5) was obtained from the literature or from visual inspection of our spectra. Column 10 shows the estimate of the star's average mean field modulus $\langle |B| \rangle$ obtained as explained by Bagnulo & Landstreet (2021); a zero value means that field was not detected even with polarimetric techniques. Literature (identified thanks to the SIMBAD database) and observatory archives were searched for field detection to complement our new dataset of observations of WDs – references to field measurements are given in col. 11. The Montreal White Dwarf Database (Dufour et al. 2017) was also used for the analysis of various individual stars. We note that in the previous 20 pc volume survey by Bagnulo & Landstreet (2021), stellar parameters were estimated using the various modelling results available in the literature,

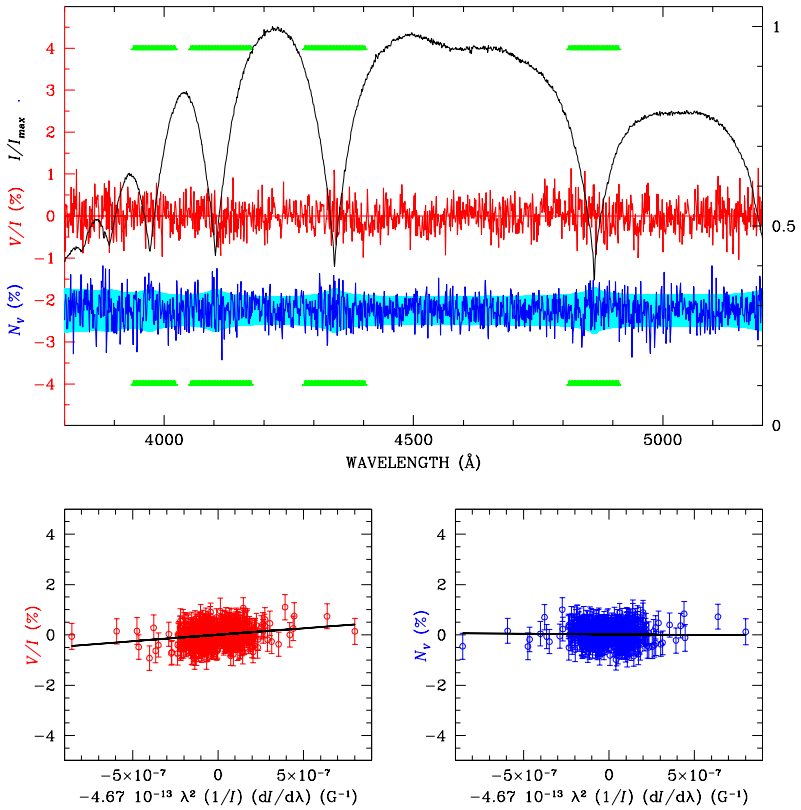

Figure 5. Same as for Fig. 4, for the weakly magnetic star WD 0232+525 = EGGR 314, observed with the blue arm of ISIS. Note the shorter range of the x-axis, with respect to Fig. 4, due to the fact that the Balmer lines of the WD are much broader than those of the main sequence Ap star HD 94660.

many of which pre-dated Gaia. These data have been revised as explained above, therefore some parameters reported in Table 2 may slightly differ from those given in Table 2 of Bagnulo & Landstreet (2021).

In our compilation we found it useful to stick to a simple and homogeneous nomenclature of the stars, and in col. 1 of both Table 1 and 2 we use the naming system based on 1950 coordinates created at the Villanova University, which was originally introduced by McCook & Sion (1977), and more explicitly defined by McCook & Sion (1999) as "WD" followed by the first four digits of the right ascension, the sign of the declination, the first two digits of the declination, and a third digit in which minutes of declination are expressed as the truncated fraction of degree. Some names were given incorrectly in the past, frequently because the third digit of declination was rounded instead of being truncated, but we have not changed that name if it had been already used in previous literature. Many stars of Table 2 have been baptised in the Villanova system for the first time in this work, and the Simbad main identifier can be found in col. 2 of Table 2. Magnetic WDs are identified with the symbol "H" in their spectral classification of col. 3.

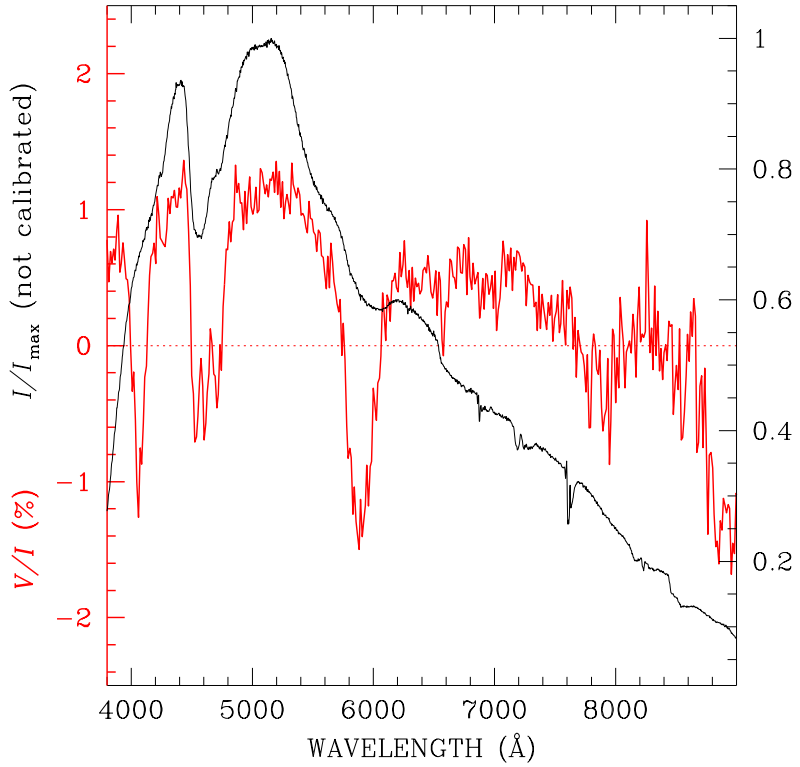

Figure 6. FORS2 observations of WD 1008−242 obtained with grism 300V. The black solid line shows the non-calibrated flux, normalised to its maximum value (scale on the right y-axis) and the red solid line is the circular polarisation expressed in percent (scale on the left y-axis).

Table 1. New magnetic field measurements of young WDs between 20 and 40 pc.

STAR	INSTRUMENT	Grism/ Grating	DATE yyyy-mm-dd	UT hh:mm	Exp (s)	S/N $Å^{-1}$	$\langle B_z \rangle$ (kG)
WD 0000−170	FORS2	600B	2021-08-21	04:45	3000	485	−2.58±1.20
WD 0002+729	ISIS	R600B	2019-10-12	00:14	3600	215	2.29±1.12
		R1200R				165	−0.58±1.05
WD 0125+135	FORS2	1200R	2021-08-22	05:08	2800	400	−0.64±0.71
	ESPaDOnS		2021-11-29	05:03	2800	34	−4.40±3.84
WD 0126+508	ESPaDOnS		2021-08-29	13:16	3000	145	0.06±1.10
WD 0133−116	FORS2	1200R	2021-08-23	04:37	2800	440	0.25±0.70
WD 0134+833	ESPaDOnS		2016-10-14	08:39	3360	170	−0.82±0.57
WD 0145+234	ISIS	R600B	2019-10-07	01:53	3600	320	−0.37±1.05
		R1200R				230	1.56±0.83
WD 0205+250	ESPaDOnS		2015-11-02	09:26	4620	264	1.01±0.64
WD 0214+568	ESPaDOnS		2021-08-31	10:08	3600	139	−0.84±1.0
WD 0227+050	ESPaDOnS		2016-08-13	14:53	3360	212	1.12±0.45
WD 0231+570	ISIS	R600B	2019-10-07	03:04	3600	310	−0.86±1.13
		R1200R				220	−0.55±0.53
WD 0232+525	ISIS	R600B	2019-10-08	10:10	3600	335	5.02±1.22
		R1200R				230	2.72±1.69
	ISIS	R600B	2019-10-10	02:02	3600	295	3.82±1.47
		R1200R				205	4.25±0.99
	ESPaDOnS		2021-11-27	05:14	4200	155	−5.60±1.40
WD 0311−563	FORS2	1200B	2021-08-23	05:48	3000	455	2.02±0.78
WD 0311−649	FORS2	1200B	2021-08-21	06:56	2700	720	−0.16±0.31
WD 0325−857	FORS2	1200R	2021-08-22	04:06	2800	430	0.32±0.58
WD 0342+195	ESPaDOnS		2022-02-21	06:40	5200	150	−2.04±0.97
WD 0343+438	ESPaDOnS		2021-08-27	11:35	4200	152	0.24±0.67
WD 0352+096	FORS2	1200R	2021-09-06	06:47	3000	440	0.14±0.49
WD 0401+250	ESPaDOnS		2017-02-05	0522	3260	124	0.47±0.87
WD 0407+179	FORS2	1200R	2021-09-02	09:02	2800	490	1.06±0.49
	ESPaDOnS		2021-11-29	08:39	4800	69	3.43±1.28
WD 0426−049	FORS2	1200R	2021-08-23	08:16	3000	445	0.11±0.61
WD 0453+418	ESPaDOnS		2017-02-15	09:46	3260	110	−0.70±0.72
WD 0503+147	ISIS	R600B	2019-10-08	05:45	3600	210	−1.05±0.99
		R1200R				155	1.67±1.83
	FORS2	1200B	2021-12-14	02:27	2800	610	0.40±0.39
WD 0522−056	FORS2	1200R	2021-08-26	09:23	2800	550	−0.27±0.44
WD 0615−591	FORS2	600B	2021-08-24	08:36	2800	415	0.51±0.55
WD 0622−801	FORS2	1200R	2021-09-02	06:39	3000	320	2.14±1.17
WD 0700+256	ESPaDOnS		2022-02-21	08:08	3600	169	−0.80±9.74
WD 0732−427	FORS2	1200R	2021-11-20	05:53	5600	420	−1.17±0.83
	FORS2	1200R	2021-12-12	03:30	5600	380	0.23±1.14
WD 0743+442	ESPaDOnS		2022-02-21	09:40	7060	112	0.79±1.01
WD 0752−146	ESPaDOnS		2017-01-14	12:29	3260	102	0.88±0.94
	ESPaDOnS		2017-02-14	03:18	3260	147	0.39±0.76
WD 0809+177	ESPaDOnS		2018-02-04	02:32	2268	68	0.24±1.94
WD 0823−073	FORS2	1200R	2021-12-15	06:44	2800	530	0.39±0.50
WD 0836−501	FORS2	1200B	2021-12-12	05:44	3000	495	0.40±0.90

Table 1. continued.

STAR	INSTRUMENT	Grism/ Grating	DATE yyyy-mm-dd	UT hh:mm	Exp (s)	S/N Å^{-1}	$\langle B_z \rangle$ (kG)
	FORS2	1200B	2021-12-13	04:57	3000	470	−0.17±0.92
WD 0858+363	ESPaDOnS		2022-02-22	09:24	7060	178	0.52±0.96
	ESPaDOnS		2022-02-23	12:27	7060	137	−0.73±1.45
WD 0943+441	ESPaDOnS		2016-01-17	13:52	4620	196	−0.00±0.46
	ESPaDOnS		2016-01-25	11:46	3400	127	−1.84±0.85
	ESPaDOnS		2016-10-19	15:12	3360	156	−0.47±0.37
	ESPaDOnS		2016-12-21	15:48	3360	170	0.11±0.46
WD 0954−710	FORS2	1200R	2021-12-14	05:33	2700	620	−0.05±0.60
WD 1005+642	ESPaDOnS		2018-01-30	10:46	2268	90	−1.76±1.48
WD 1008−242	FORS2	600B	2022-01-01	06:59	3000	370	$\lvert V/I \rvert \sim 1.5\,\%$
	FORS2	300V	2022-02-10	01:12	1800	290	$\lvert V/I \rvert \sim 1.5\,\%$
WD 1026+023	FORS2	1200R	2022-02-11	03:50	2800	480	0.27±0.74
WD 1032−671	FORS2	1200R	2021-12-14	06:32	2700	590	0.32±0.61
	FORS2	1200R	2021-12-18	05:56	2700	610	0.22±0.45
WD 1049−158	FORS2	1200R	2021-12-15	07:42	2800	370	−1.51±0.77
	FORS2	1200R	2022-01-19	05:49	2800	485	−0.76±0.60
WD 1052+273	ISIS	R600B	2019-04-20	22:46	3600	260	1.75±1.77
		R1200R				130	−1.55±1.05
	ESPaDOnS		2018-02-04	12:27	3468	75	−5.45±2.30
	ESPaDOnS		2018-02-07	13:07	3468	69	−2.25±2.24
WD 1053−550	FORS2	1200R	2022-01-13	07:06	2800	550	0.30±0.43
WD 1104+602	ESPaDOnS		2017-01-16	13:56	3260	113	−1.61±0.84
WD 1143+321	ESPaDOnS		2017-01-12	12:24	3260	118	−1.00±0.81
	ESPaDOnS		2018-02-01	13:28	2268	50	−1.13±1.42
WD 1225−079	FORS2	1200B	2021-12-18	07:58	3000	445	0.65±0.91
WD 1229−503	FORS2	600B	2022-01-18	06:34	2700	560	−0.37±0.84
WD 1310+583	ESPaDOnS		2018-02-07	14:11	3468	68	−0.18±2.61
WD 1319+466	ESPaDOnS		2017-05-14	08:54	4800	114	0.62±1.05
WD 1322−599	FORS2	1200R	2021-08-22	00:18	3000	345	−1.52±3.16
WD 1333+487	ESPaDOnS		2022-02-17	14:57	5200	161	−0.45±0.69
WD 1337+705	ESPaDOnS		2017-01-22	13:54	3260	195	0.05±0.63
	ESPaDOnS		2017-03-04	10:14	3260	240	0.00±0.47
WD 1344+572	ISIS	R600B	2019-04-20	23:27	2400	265	1.52±1.47
		R1200R				130	0.85±0.67
	ESPaDOnS		2019-03-18	13:09	4148	202	−0.12±0.52
	ESPaDOnS		2019-06-10	08:05	4188	200	0.05±0.48
WD 1443+295	ESPaDOnS		2022-02-20	12:48	7060	148	2.20±0.99
WD 1509+322	ESPaDOnS		2018-02-07	15:14	3468	55	−0.47±2.86
			2022-02-17	09:03	6200	155	−0.16±0.56
WD 1511−200	ESPaDOnS		2022-02-20	14:28	4320	134	−1.6±1.24
WD 1544+380	ESPaDOnS		2021-08-27	06:12	7060	164	−0.16±0.62
WD 1546−398	FORS2	600B	2022-04-09	08:13	2400	385	−0.32±0.90
WD 1559+369	ESPaDOnS		2021-08-31	05:58	5600	154	−2.06±1.09
WD 1601+581	ESPaDOnS		2018-06-22	06:10	3468	137	0.48±0.58
WD 1704+481.1	ESPaDOnS	(SB2)	2022-02-21	15:03	5600	162	−6.39±1.01
WD 1704+481.2	ESPaDOnS	(SB2)	2021-09-02	07:08	5600	162	6.46±4.18

Table 1. continued.

STAR	INSTRUMENT	Grism/ Grating	DATE yyyy-mm-dd	UT hh:mm	Exp (s)	S/N $Å^{-1}$	$\langle B_z \rangle$ (kG)
WD 1713+695	ESPaDOnS		2017-02-04	15:36	3260	175	1.25±0.65
WD 1716+020	ESPaDOnS		2022-07-12	11:16	6200	145	−0.08±0.65
WD 1752−249	FORS2	1200R	2021-06-09	07:33	2400	310	−0.53±1.19
WD 1752+331	ESPaDOnS		2021-08-27	09:47	3600	130	−1.13±0.75
WD 1807+299	ISIS	R600B	2019-04-21	03:12	2400	310	3.71±1.51
		R1200R					2.89±1.34
WD 1911+536	ESPaDOnS		2018-06-21	08:28	1668	112	0.89±0.83
WD 1911+135	ESPaDOnS		2022-07-11	11:34	5220	150	−0.54±0.63
WD 1916−362	FORS2	1200R	2018-05-26	06:55	2700	675	−0.96±0.62
WD 1927+112	ESPaDOnS		2021-09-02	08:25	3000	167	0.54±0.78
WD 1934+264	ISIS	R600B	2019-10-07	21:43	3600	365	0.89±1.31
		R1200R				235	−0.38±0.58
	ISIS	R600B	2019-10-10	22:48	3600	315	2.95±1.51
‘		R1200R				235	−1.36±1.36
	ESPaDOnS		2019-06-09	12:35	3400	200	1.11±0.65
WD 2040−392	FORS2	1200R	2018-05-26	09:31	2700	635	−0.75±0.54
WD 2118−262	ESPaDOnS		2019-11-15	06:28	2268	180	−0.21±0.67
WD 2126+734	ESPaDOnS		2015-10-31	05:05	3256	260	0.26±0.40
WD 2136+828	ESPaDOnS		2016-06-10	14:29	3400	172	−0.24±0.57
WD 2133−135	ISIS	R600B	2019-10-07	22:51	3600	245	−0.56±1.21
		R1200R					0.00±1.13
WD 2147+280	ESPaDOnS		2021-08-29	11:41	7060	164	0.35±0.48
WD 2149+021	ESPaDOnS		2015-10-31	07:06	3256	268	0.39±0.36
WD 2210+565	ESPaDOnS		2018-06-30	14:42	1368	44	2.13±2.88
	ESPaDOnS		2018-07-02	14:17	3468	87	2.81±1.13
	ESPaDOnS		2018-10-02	09:42	2268	57	0.86±1.38
WD 2305−220	FORS2	1200R	2021-08-26	08:25	2800	580	−0.08±0.45
WD 2307−691	FORS2	600B	2021-08-21	01:01	2700	275	$\lvert V/I \rvert \leq 0.05\,\%$
WD 2316−173	ISIS	R600B	2019-10-08	21:25	3600	210	10.0±12.0
		R1200R				170	$\lvert V/I \rvert \leq 0.20\,\%$
% WD 2329+407	ESPaDOnS		2021-08-29	10:02	4200	163	−0.52±0.63
WD 2333−165	FORS2	1200R	2021-08-21	03:47	2700	670	0.00±0.37

Table 2. Physical parameters of the WDs checked for magnetic field in the context of a volume-limited survey.

STAR	Spectral Class	G	ATM	$T_{\rm eff}$ (K)	M ($M_\odot$)	Age (Gyr)	d (pc)	$\overline{\langle\|B\|\rangle}$ (MG)	References
WD 2359−434	LAWD 96	DAH	12.9	H	8428	0.82	1.774	8.3	0.10	B&L21
WD 0000−345	LAWD 1	DC	14.9	He	6332	0.66	2.86	14.8	0	B&L21
WD 0000−170	EGGR 508	DB	14.6	He	12868	0.62	0.36	38.1	0	Ftw
WD 0002+729	GD 408	DBZ	14.3	He	13788	0.63	0.30	34.5	0	Itw
WD 0004+122	LP 464-57	DCH	16.3	He	5098	0.69	6.80	17.5	100	B&L21
WD 0009+501	EGGR 381	DAH	14.2	H	6483	0.74	3.23	10.9	0.25	B&L21
WD 0011−721	L 50-73	DAH	15.0	H	6275	0.52	1.72	18.8	0.37	B&L21
WD 0011−134	G 158-45	DAH	15.8	H	5871	0.72	4.18	18.6	12	B&L21
WD 0038−226	EGGR 246	DQpec	14.3	He	5368	0.56	4.55	9.1	0	B&L21
WD 0041−102	Feige 7	DBAH	14.5	He	21341	1.14	0.35	31.1	20	Lie+77
WD 0046+051	Wolf 28	DZ	12.3	He	6455	0.74	3.48	4.3	0	B&L21
WD 0115+159	Wolf 1516	DQ	13.8	He	9693	0.71	0.96	16.8	0	B&L21
WD 0121−429A	LP 991-16	DAH	14.7	H	6035	0.69	3.44	18.5	5.5	B&L21
WD 0121−429B	LP 991-16	DC	14.7	He	6035	0.69	3.86	18.5	0	B&L21
WD 0123−262	EGGR 307	DC	15.0	He	7204	0.80	2.94	16.6	0	B&L21
WD 0125+135	CHSS 3246	DA	14.3	H	13094	0.56	0.27	37.6	0	Ftw, Etw
WD 0126+508	GD 277	DA	13.5	H	22090	0.63	0.04	38.4	0	Etw
WD 0126+101	Wolf 72	DA	14.4	H	8516	0.39	0.59	29.3	0	S&S95
WD 0133−116	V* ZZ Cet	DA	14.2	H	11832	0.57	0.37	32.7	0	Ftw
WD 0135−052A	LAWD 10	DA	12.7	H	7470	0.47	0.99	12.6	0	B&L21
WD 0135−052B	LAWD 10	DA	12.7	H	6920	0.52	1.35	12.6	0	B&L21
WD 0134+833	GD 419	DA	13.1	H	19003	0.65	0.09	27.1	0	B&L18, Etw
WD 0141−675	L 88-59	DAZ	13.7	H	6350	0.58	1.96	9.7	0	B&L21
WD 0142+312	EGGR 519	DA	14.7	H	8965	0.41	0.54	36.6	0	S&S95
WD 0145+234	WD 0145+234	DA	14.0	H	12989	0.66	0.35	29.4	0	Itw
WD 0148+641	EGGR 268	DA	13.9	H	8794	0.66	1.00	17.3	0	B&L21
WD 0148+467	GD 279	DA	12.5	H	14291	0.61	0.24	16.5	0	B&L21
WD 0205+250	LAWD 11	DA	13.2	H	16931	0.41	0.06	39.1	0	S&S95, B&L18, Etw
WD 0208−510	HD 13445B	DQ	13.1	He	8180	0.59	1.25	10.8	0	B&L21
WD 0208+396	EGGR 168	DAZ	14.4	H	7196	0.55	1.33	17.2	0	B&L21
WD 0210−083	LP 649-67	DA	13.7	H	8467	0.53	0.84	16.7	0	B&L21
WD 0214+568	LAWD 12	DA	13.6	H	22260	0.64	0.04	39.7	0	S&S95, Etw
WD 0227+050	Feige 22	DA	12.8	H	18963	0.55	0.06	26.5	0	Azn04, Etw
WD 0230−144	EGGR 471	DA	15.6	H	5393	0.57	3.35	16.7	0	B&L21
WD 0233−242A	LP 830-14	DAH	15.7	H	4875	0.66	8.07	18.5	3.8	B&L21
WD 0233−242B	LP 830-14	DC?	15.7	He?	4875	0.66	7.06	18.5	0	B&L21
WD 0231+570	GD 283	DA	13.8	H	12657	0.63	0.36	26.7	0	Itw
WD 0232+525	EGGR 314	DAH	13.9	H	17350	0.82	0.23	28.8	0.01	B&L21, Itw, Etw
WD 0245+541	EGGR 473	DAZ	15.1	H	4942	0.59	6.53	10.9	0	B&L21
WD 0301+059	SDSS J030350.63+060748.9	DAH	15.0	H	20823	1.18	0.44	31.3	200	L&B20
WD 0302+621	GD 426	DA	15.0	H	11032	0.68	0.58	38.1	0	S&S95
WD 0310−688	CPD-69 177	DA	11.4	H	15865	0.66	0.19	10.4	0	B&L21
WD 0311−649A	WT 106	DA uDD	13.3	H	12000	0.40	0.22	36.6	0	Ftw
WD 0311−649B	WT 106	DA uDD	13.3	H	12300	0.55	0.32	36.6	0	Ftw

Table 2. continued.

STAR	Spectral Class	G	ATM	$T_{\rm eff}$ (K)	M ($M_\odot$)	Age (Gyr)	d (pc)	$\overline{\langle\|B\|\rangle}$ (MG)	References
WD 0311−563	Gaia EDR3 4733604373137759616	DA	14.6	H	10984	0.60	0.49	34.8	0	Ftw
WD 0316−849	V* CL Oct	DAH	14.8	H	26465	1.27	0.33	29.4	300	Bar+95
WD 0325−857	LB 9802	DA	14.1	H	16533	0.85	0.29	29.4	0	Kaw+07, Ftw
WD 0322−019	EGGR 566	DAZH	15.9	H	5165	0.61	5.49	16.9	0.12	B&L21
WD 0341+182	Wolf 219	DQ	15.1	He	6837	0.63	1.97	18.9	0	B&L21
WD 0342+195	Wolf 222	DA	14.2	H	12551	0.75	0.48	28.2	0	Etw
WD 0343+438	Wolf 226	DA	14.0	H	13660	0.61	0.27	31.9	0	Etw
WD 0346−011	GD 50	DA	14.0	H	39304	1.26	0.10	31.0	0	Azn+04
WD 0352+096	HZ 4	DA	14.5	H	14516	0.79	0.36	35.0	0	S&S95, Fw
WD 0357+081	G 7-16	DA	15.7	H	5461	0.54	2.76	18.6	0	B&L21
WD 0401+250	G 8-8	DA	13.8	H	12318	0.63	0.39	26.5	0	S&S95, Etw
WD 0407+179	HZ 10	DA	14.2	H	12985	0.60	0.31	34.1	0	S&S95, Etw, Ftw
WD 0413−077	* omi02 Eri B	DA	9.5	H	16265	0.57	0.13	5.0	0	B&L21
WD 0415−594	* eps Ret B	DA	12.5	H	14270	0.51	0.18	18.3	0	B&L21
WD 0423+120	EGGR 169	DC	15.3	He	6153	0.71	3.74	16.0	0	B&L21
WD 0426−049	HE 0426-0455	DA	14.5	H	14099	0.64	0.27	39.3	0	Ftw
WD 0426+588	EGGR 180	DC	12.3	He	7294	0.72	2.19	5.5	0	B&L21
WD 0433+270	HD 283750B	DA	15.6	H	5534	0.60	3.23	17.4	0	B&L21
WD 0435−088	EGGR 41	DQ	13.6	He	6601	0.60	2.02	9.4	0	B&L21
WD 0453+418	GD 64	DA	14.0	H	14266	0.49	0.17	38.1	0	S&S95, Etw
WD 0503−174	LP 777-1	DAH	15.8	H	5345	0.50	2.69	19.3	4.3	B&L21
WD 0503+147	KUV 05034+1445	DB	14.1	He	15345	0.57	0.18	38.6	0	Itw, Ftw
WD 0522−056	UCAC4 423-009416	DA	13.9	H	17078	0.62	0.13	35.7	0	Ftw
WD 0548−001	EGGR 248	DQH	14.4	He	6053	0.65	3.35	11.2	5	B&L21
WD 0552−106	UCAC4 398-010797	DZ	14.9	He	6578	0.68	2.71	15.3	0	B&L21
WD 0552−041	EGGR 45	DZ	14.2	He	4822	0.64	7.00	6.4	0	B&L21
WD 0553+053	EGGR 290	DAH	14.0	H	5729	0.68	3.96	8.1	15	B&L21
WD 0615−591	WG 8	DB3+	14.0	He	15457	0.58	0.18	36.1	0	Ftw
WD 0622−801	EC 06220-8010	DA	14.9	H	13396	0.86	0.53	35.7	0	Ftw
WD 0642−166	* alf CMa B	DA	8.5	H	10896	0.44	0.34	2.7	0	B&L21
WD 0644+025	EGGR 484	DA	15.6	H	7109	0.97	4.31	18.1	0	B&L21
WD 0644+375	LAWD 23	DA	12.1	H	21393	0.71	0.07	17.1	0	B&L21
WD 0655−390	L 454-9	DA	15.0	H	6369	0.64	2.26	16.5	0	B&L21
WD 0657+320	EGGR 485	DA	16.3	H	4873	0.52	5.44	19.6	0	B&L21
WD 0700+256	UCAC4 578-037125	DBA	13.9	He	11675	0.58	0.43	25.6	0	Etw
WD 0708−670	SCR J0708-6706	DCH	16.0	He	4847	0.48	4.95	17.0	200	B&L21
WD 0727+482A	EGGR 52A	DA	15.3	H	5225	0.63	5.47	11.1	0	B&L21
WD 0727+482B	EGGR 52B		15.6	H	4775	0.60	7.56	11.1	0	B&L21
WD 0728+642	EGGR 321	DA H?	16.0	H	5140	0.48	3.06	20.0	0	B&L21
WD 0732−427	LAWD 24	DA	14.2	H	15030	0.70	0.26	33.7	0	Ftw
WD 0736+053	alf CMi B = Procyon B	DQZ	10.9	He	7585	0.55	1.25	3.5	0	B&L21
WD 0738−172	LAWD 25	DZA H?	13.0	He	7982	0.66	1.41	9.1	0	B&L21
WD 0743−336	VB 3	DC	16.3	H	4293	0.46	6.58	15.4	0	B&L21
WD 0743+442	GD 89	DA	14.9	H	15196	0.89	0.40	38.3	0	Etw
WD 0747+073.1	EGGR 426	DC	16.6	H	4281	0.46	6.68	18.2	0	B&L21
WD 0747+073.2	EGGR 427	DC	16.3	H	4680	0.51	6.20	18.1	0	B&L21

Table 2. continued.

STAR	Spectral Class	G	ATM	$T_{\rm eff}$ (K)	M ($M_\odot$)	Age (Gyr)	d (pc)	$\overline{\langle\|B\|\rangle}$ (MG)	References
WD 0752−676	LAWD 26	DA	H	13.8	5630	0.55	2.56	8.2	0	B&L21
WD 0751−252	SCR J0753-2524	DA	H	16.0	4939	0.52	4.90	17.8	0	B&L21
WD 0752−146	EGGR 57	DA+dMe	H	13.6	19400	0.58	0.06	39.1	0	S&S95, Etw
WD 0806−661	L 97-3	DQ	He	13.7	10721	0.66	0.65	19.2	0	B&L21
WD 0810−353	UPM J0812-3529	DAH	H	14.3	6239	0.70	3.16	11.2	30	B&L21
WD 0809+177	PM J08126+1737	DA	H	13.4	16027	0.64	0.18	27.0	0	Etw
WD 0810+489	G 111-64	DC	He	14.9	6709	0.65	2.17	17.1	0	B&L21
WD 0816−310	SCR J0818-3110	DZH	He	15.4	6754	0.74	3.03	19.4	0.09	B&L21
WD 0821−669	SCR J0821-6703	DA	H	15.1	4793	0.52	5.75	10.7	0	B&L21
WD 0823−073	UCAC4 413-046149	DA	H	14.0	15369	0.58	0.17	35.5	0	Ftw
WD 0836−501	UPM J0837-5017	DA	H	14.6	12484	0.80	0.56	31.7	0	Ftw
WD 0839−327	CD-32 5613	DA	H	11.8	9086	0.47	0.61	8.5	0	B&L21
WD 0840−136	LP 726-1	DZ	He	15.6	5388	0.68	5.89	14.8	0	B&L21
WD 0856−007	LP 606-32	DAZ	H	16.1	4997	0.55	5.22	18.3	0	B&L21
WD 0858+363	V* VW Lyn	DA	H	14.6	11719	0.67	0.48	34.0	0	Etw
WD 0859−039	RE J090217-040712	DA	H	13.2	23798	0.56	0.02	37.9	0	Azn+04, Kaw+07, B&L18
WD 0912+536	EGGR 250	DCH	He	13.8	7454	0.79	2.63	10.3	100	B&L21
WD 0943+441	LAWD 32	DA	H	13.3	13820	0.42	0.15	32.0	0	B&L18, Etw
WD 0945+245	PG 0945+246	DAH (DD?)	H	14.3	17919	0.90	0.20	36.2	670	Lie+93
WD 0954−710	L 64-27	DA	H	13.5	14274	0.50	0.17	30.6	0	Ftw
WD 0959+149	EGGR 252	DC	He	15.3	6779	0.70	2.63	19.4	0	B&L21
WD 1005+642	GD 462	DA	H	13.7	19684	0.60	0.06	39.4	0	Etw
WD 1008−242	UCAC4 328-061594	DAH? DQH?	H	15.2	21652	1.15	0.34	39.7	150	**Ftw**
WD 1008+290	LP 315-42	DQpecH	He	16.5	3962	0.41	5.99	14.7	300	B&L21
WD 1009−184	WT 1759	DZH	He	15.3	6394	0.69	3.04	18.1	0.15	B&L21
WD 1019+637	EGGR 350	DA	H	14.6	6801	0.61	1.77	15.9	0	B&L21
WD 1026+023	PG 1026+024	DA	H	14.3	12611	0.61	0.35	33.6	0	Ftw
WD 1031−114	EGGR 70	DA	H	13.0	25387	0.60	0.02	35.7	0	S&S95, B&L18
WD 1032−671	UCAC4 114-031850	DA	H	13.4	18778	0.86	0.20	23.6	0	Ftw
WD 1033+714	LP 37-186	DC	H	16.6	4693	0.68	9.01	17.6	0	B&L21
WD 1036−204	EGGR 535	DQpecH	He	15.8	5754	0.94	6.19	14.1	265	B&L21
WD 1042−690	WG 17	DA+dM	H	12.7	21000	0.50	0.03	29.3	0	Azn+04
WD 1043−188	BD-18 3019B	DQpec	He	15.4	5736	0.50	2.52	18.8	0	B&L21
WD 1049−158	HE 1049-1552	DA	H	14.4	19295	0.85	0.18	38.7	0	Ftw
WD 1052+273	Ton 556	DA	H	14.1	22501	0.86	0.11	37.8	0	S&S95, Itw, Etw
WD 1053−550	LAWD 33	DA	H	14.2	14225	0.61	0.24	35.4	0	Ftw
WD 1055−072	LAWD 34	DC	He	14.2	7388	0.81	2.82	12.3	0	B&L21
WD 1104+602	EGGR 75	DA	H	13.8	18319	0.69	0.13	34.5	0	S&S95, Etw
WD 1105−340	SCR J1107-3420A	DAH+dM	H	13.7	13602	0.66	0.31	26.2	0.15	L&B19
WD 1105−048	EGGR 76	DAH+dM	H	13.1	15701	0.57	0.15	24.8	0.01	Azn+04, B&L18
WD 1116−470	SCR J1118-4721	DC H?	He	15.4	5910	0.62	3.40	17.0	0	B&L21
WD 1116+026	GD 133	DAZ	H	14.6	12157	0.63	0.40	38.2	0	B&L18
WD 1121+216	Ross 627	DA	H	14.1	7373	0.61	1.45	14.7	0	B&L21
WD 1132−325	* 20 Crt B	DC	H	14.5	5420	0.66	4.90	9.6	0	B&L21
WD 1134+300	GD 140	DA	H	12.5	21336	0.94	0.17	15.7	0	B&L21
WD 1142−645	LAWD 37	DQ	He	11.4	8429	0.71	1.37	4.6	0	B&L21

Table 2. continued.

STAR	Spectral Class	G	ATM	$T_{\rm eff}$ (K)	M ($M_\odot$)	Age (Gyr)	d (pc)	$\overline{\langle\|B\|\rangle}$ (MG)	References
WD 1143+321	EGGR 185	DA	13.7	H	15733	0.61	0.17	31.3	0	S&S95, Etw
WD 1145−747	SSSPM J1148-7458	DC	17.2	H	3821	0.44	7.62	20.0	0	B&L21
WD 1148+687	PM J11508+6831	DA	15.1	H	6696	0.75	3.05	17.1	0	B&L21
WD 1202−232	LP 852-7	DAZ	12.7	H	8540	0.57	0.89	10.4	0	B&L21
WD 1208+576	G 197-47	DAZ	15.6	H	5829	0.58	2.44	20.0	0	B&L21
WD 1223−659	WG 21	DAZ	13.9	H	7582	0.53	1.11	15.4	0	B&L21
WD 1225−079	PG 1225-079	DZA	14.7	He	11727	0.76	0.62	32.7	0	Ftw
WD 1229−502	UCAC4 198-073015	DA	13.5	H	18011	0.58	0.09	32.8	0	Ftw
WD 1236−495	WG 22	DA	13.8	H	11359	1.04	1.57	14.8	0	B&L21
WD 1257+037	Wolf 457	DA	15.6	H	5650	0.70	4.57	16.5	0	B&L21
WD 1309+853	EGGR 436	DAH	15.8	H	5254	0.63	5.27	16.5	5.4	B&L21
WD 1310−472	NAME ER 8	DC	16.7	H	3855	0.42	7.10	16.8	0	B&L21
WD 1310+583	PG 1310+583	DA	14.1	H	10312	0.45	0.41	30.8	0	S&S95, Etw
WD 1316−215	LP 854-50	DA	16.5	H	5882	0.99	6.33	19.8	0	B&L21
WD 1315−781	LAWD 45	DAH	16.0	H	5542	0.66	4.35	19.3	5.6	B&L21
WD 1319+466	PG 1319+466	DA	14.5	H	14625	0.84	0.40	32.9	0	S&S95, Etw
WD 1322−599	Gaia EDR3 5869567658943170048	DBA	14.8	H	11506	0.68	0.53	35.9	0	Ftw
WD 1327−083	BD-07 3632	DA	12.4	H	14562	0.59	0.21	16.1	0	B&L21
WD 1333+487	GD 325	DB	14.1	He	14575	0.54	0.20	36.9	0	Etw
WD 1334+039	Wolf 489	DA	14.4	H	4858	0.48	4.42	14.7	0	B&L21
WD 1337+705	LAWD 52	DB	12.8	He	21478	0.64	0.06	26.5	0	S&S95, B&L18, Etw
WD 1338+052	LSPM J1341+0500	DC	16.3	H	4022	0.44	7.09	14.7	0	B&L21
WD 1344+572	PG 1344+573	DA	13.5	H	14093	0.64	0.27	25.0	0	S&S95, Itw, Etw
WD 1345+238	EGGR 438	DA	15.3	H	4576	0.46	5.40	11.9	0	B&L21
WD 1350−090	PG 1350-090	DAH	14.5	H	8881	0.80	1.41	19.7	0.45	B&L21
WD 1408−591	VVV J141159.32-592045.7	DA	14.6	H	6653	0.66	2.12	14.4	0	B&L21
WD 1422+095	GD 165	DA	14.3	H	12390	0.64	0.39	33.3	0	B&L18
WD 1425−811	V* MY Aps	DA	13.4	H	12146	0.67	0.45	20.9	0	Lan+12
WD 1443+295	Ton 213	DA	14.5	H	12443	0.58	0.34	38.4	0	Etw
WD 1444−174	LP 801-9	DA	16.2	H	4980	0.87	9.62	13.3	0	B&L21
WD 1508+637	GD 340	DA	14.7	H	10317	0.57	0.55	34.8	0	S&S95
WD 1509+322	GD 178	DA	14.1	H	14770	0.66	0.25	34.2	0	S&S95, Etw
WD 1511−200	Gaia EDR3 6255777749623059584	DA	14.1	H	10902	0.59	0.49	27.6	0	Etw
WD 1532+129	G 137-24	DZH	15.6	He	5790	0.56	2.96	19.3	0.05	B&L21
WD 1544+380	HS 1544+3800	DA	14.5	H	13288	0.64	0.32	37.5	0	Etw
WD 1544−377	HD 140901B	DA	13.0	H	10392	0.62	0.59	15.2	0	B&L21
WD 1546−397	UCAC4 251-083082	DB	14.4	He	13358	0.57	0.28	37.8	0	Ftw
WD 1550+183	GD 194	DA	14.8	H	14811	0.86	0.41	36.9	0	S&S95
WD 1559+369	Ross 808	DA	14.4	H	11119	0.59	0.46	32.8	0	S&S95, Etw
WD 1601+581	PG 1601+581	DA	13.8	H	15563	0.61	0.18	32.4	0	S&S95, Etw
WD 1620−391	CD-38 10980	DA	11.0	H	24073	0.64	0.03	12.9	0	B&L21
WD 1626+368	Ross 640	DZA	13.8	He	9381	0.72	1.06	15.9	0	B&L21
WD 1630+089	G 138-38	DA	14.9	H	5594	0.59	3.00	12.9	0	B&L21
WD 1633+572	EGGR 258	DQ	14.8	He	6126	0.58	2.43	14.8	0	B&L21
WD 1632+177A	PG 1632+177	DAZ	13.1	H	8900	0.40	0.54	25.6	0	S&S95, B&L18
WD 1632+177B	PG 1632+177	DAZ	13.1	H	11200	0.53	0.40	25.6	0	S&S95, B&L18

Table 2. continued.

STAR		Spectral Class	G	ATM	$T_{\rm eff}$ (K)	M ($M_\odot$)	Age (Gyr)	d (pc)	$\overline{\langle\|B\|\rangle}$ (MG)	References
WD 1633+433	PG 1633+434	DAZ	14.7	H	6516	0.68	2.53	14.5	0	B&L21
WD 1647+591	V* DN Dra	DA	12.3	H	12181	0.78	0.57	10.9	0	B&L21
WD 1658+440	PG 1658+441	DAH	14.8	H	29612	1.28	0.28	31.7	1.32	Sch+92
WD 1659−531	WG 32	DA	13.5	H	15050	0.65	0.22	26.7	0	Kaw+07
WD 1704+481.2	EGGR 577	DA uDD	14.4	H	9500	0.39	0.53	39.4	0	Etw
WD 1704+481.1	EGGR 576	DA H?	14.5	H	14222	0.66	0.27	39.5	0.01	Etw
WD 1703−267	UCAC4 317-104829	DAH	15.0	H	6128	0.81	4.61	13.0	8	B&L21
WD 1705+030	EGGR 494	DZ	15.1	He	6927	0.73	2.67	17.8	0	B&L21
WD 1713+695	EGGR 370	DA	13.3	H	15732	0.61	0.17	26.3	0	B&L18, Etw
WD 1716+020	Wolf 672 A	DA	14.4	H	12683	0.56	0.30	38.2	0	S&S95, Etw
WD 1743−132	EGGR 175	DA	14.6	H	11900	0.57	0.37	38.8	0	S&S95
WD 1743−545	PM J17476-5436	DZA	15.9	H	4358	0.47	6.63	13.5	0	B&L21
WD 1748+708	EGGR 372	DQH	13.8	He	5137	0.61	5.88	6.2	300	B&L21
WD 1752−249	Gaia EDR3 4067477554248982528	DA	14.9	H	13000	0.79	0.48	37.6	0	Ftw
WD 1756+827	EGGR 199	DA	14.2	H	7188	0.52	1.22	16.3	0	B&L21
WD 1752+331	UCAC4 616-058177	DA	13.8	H	17087	0.60	0.12	35.7	0	Etw
WD 1807+299	HD 166435B	DA	13.1	H	22521	0.86	0.11	24.5	0	Itw
WD 1814+134	LSR J1817+1328	DA	15.6	H	4873	0.48	4.34	15.1	0	B&L21
WD 1820+609	G 227-28	DA	15.4	H	4823	0.46	4.21	13.7	0	B&L21
WD 1821−131	EGGR 176	DA	15.4	H	6079	0.60	2.34	19.1	0	B&L21
WD 1823+116	UCAC4 508-079937	DA	16.3	H	4883	0.51	5.11	19.6	0	B&L21
WD 1829+547	EGGR 374	DAH	15.5	H	6711	0.90	4.37	17.0	120	B&L21
WD 1900+705	LAWD 73	DAH	13.2	H	12540	1.03	1.08	12.9	200	B&L21
WD 1911+536	LP 141-26	DA	13.2	H	17189	0.79	0.22	22.2	0	Etw
WD 1911+135	G 142-B2B	DA	14.1	H	13755	0.60	0.26	33.7	0	Etw
WD 1917+386	EGGR 375	DC	14.5	He	6310	0.68	3.14	11.9	0	B&L21
WD 1916−362	SCR J1920-3611	DB	13.6	He	21952	0.68	0.06	37.1	0	Ftw
WD 1917−077	LAWD 74	DBQA	12.3	He	11110	0.65	0.59	10.5	0	B&L21
WD 1919+061	UCAC4 482-095741	DA	15.6	H	5908	0.68	3.49	18.1	0	B&L21
WD 1919+145	GD 219	DA	13.0	H	15161	0.70	0.25	19.9	0	B&L21
WD 1927+111	UCAC4 507-103823	DA	13.5	H	20414	0.59	0.05	36.6	0	Etw
WD 1934+264	RX J1936.3+2632	DA	13.7	H	24228	0.95	0.12	30.1	0	Itw
WD 1935+276	V* PY Vul	DA	13.1	H	12021	0.63	0.42	18.3	0	B&L21
WD 1953−011	LAWD 79	DAH	13.6	H	7790	0.70	1.54	11.6	0.5	B&L21
WD 2002−110	EGGR 498	DC	16.7	H	4577	0.67	9.28	17.3	0	B&L21
WD 2007−303	CD-30 17706	DA	12.3	H	15123	0.58	0.18	16.2	0	B&L21
WD 2010+310	GD 229	DBH	14.8	He	18411	1.13	0.53	30.8	1.10	Swe+74
WD 2008−600	LEHPM 2-5312	DC	15.6	He	5362	0.58	4.84	16.4	0	B&L21
WD 2017−306	EC 20173-3036	DC	13.6	He	10313	0.67	0.75	17.5	0	B&L21
WD 2032+248	HD 340611	DA	11.5	H	20144	0.59	0.05	14.8	0	B&L21
WD 2039−202	EGGR 141	DA	12.4	H	19506	0.57	0.06	21.8	0	B&L18
WD 2040−392	L 495-82	DA	13.7	H	11225	0.63	0.50	23.3	0	Ftw
WD 2039−682	EGGR 140	DA	13.3	H	16419	0.90	0.34	19.6	0	B&L21
WD 2047+372	EGGR 261	DAH	13.0	H	14709	0.79	0.35	17.6	0.06	B&L21
WD 2048+263A	G 187-8	DA?	15.4	H	5080	0.53	4.15	19.1	0	B&L21
WD 2048+263B	G 187-8	DC?	15.4	H	5080	0.53	4.15	19.1	0	B&L21

Table 2. continued.

STAR	Spectral Class	G	ATM	$T_{\rm eff}$ (K)	M ($M_\odot$)	Age (Gyr)	d (pc)	$\overline{\langle\|B\|\rangle}$ (MG)	References
WD 2049−253	UCAC4 325-215293	DCH	16.0	He	4888	0.47	4.77	18.0	25	B&L21
WD 2051−208	BPS CS 22880-0134	DAH	15.1	H	20361	1.22	0.58	31.3	0.30	Koe+98, B&L18
WD 2054−050	Ross 193B	DC	16.3	H	4416	0.50	7.07	16.2	0	B&L21
WD 2057−493	WT 765	DA	15.3	H	5118	0.53	4.06	13.3	0	B&L21
WD 2105−820	LAWD 83	DAZH	13.6	H	9914	0.75	0.92	16.2	0.04	B&L21
WD 2117+539	EGGR 378	DA	12.4	H	14784	0.55	0.18	17.3	0	B&L21
WD 2118−261	LP 873-78	DA	12.9	H	19205	0.66	0.09	24.5	0	Etw
WD 2124+550	Ross 198	DA	14.8	H	13072	0.84	0.54	33.7	0	S&S95
WD 2126+734A	G 263-3	DA	12.9	H	15126	0.55	0.16	22.2	0	S&S95, B&L18, Etw
WD 2136+828	LAWD 88	DA	13.0	H	17487	0.58	0.10	26.4	0	S&S95, B&L18, Etw
WD 2133−135	Ross 203	DA	13.7	H	9927	0.46	0.47	23.4	0	Itw
WD 2138−332	L 570-26	DZH	14.4	He	7413	0.66	1.69	16.1	0.05	B&L21
WD 2140+207	EGGR 148	DQ	13.2	He	8893	0.73	1.24	11.0	0	B&L21
WD 2140−072	PHL 1716	DA	14.5	H	8905	0.87	1.78	18.2	0	B&L21
WD 2147+280	G 188-27	DB	14.6	He	12003	0.62	0.44	34.7	0	Etw
WD 2150+591	UCAC4 747-070768	DAH	14.4	H	5105	0.57	5.04	8.5	0.80	B&L21
WD 2149+021	EGGR 150	DA	12.8	H	17507	0.61	0.11	22.6	0	Jor+07, Etw
WD 2153−512	WG 39	DQH	14.5	He	6549	0.55	1.84	14.9	1.30	B&L21
WD 2159−754	V* CD Oct	DA	15.0	H	8875	1.00	2.75	19.0	0	B&L21
WD 2210+565	G 233-2	DA	14.1	H	16831	0.66	0.16	37.8	0	Etw
WD 2211−392	[OHD2001] WD J2214-390	DA	15.8	H	6063	0.81	4.80	18.2	0	B&L21
WD 2226−755	SSSPM J2231-7515	DC	16.4	H	3911	0.44	7.23	15.0	0	B&L21
WD 2226−754	SSSPM J2231-7514	DC	16.2	H	4194	0.44	6.44	15.0	0	B&L21
WD 2246+223	EGGR 155	DA	14.4	H	10534	1.02	1.85	17.8	0	B&L21
WD 2248+293A	EGGR 283	DA	15.3	H	5610	0.74	4.74	20.0	0	B&L21
WD 2248+293B	EGGR 283	DA	15.3	H	5610	0.74	4.74	20.0	0	B&L21
WD 2251−070	EGGR 453	DZ	15.4	He	4263	0.60	7.60	8.5	0	B&L21
WD 2305−220	G 275-8	DA	13.8	H	16049	0.61	0.16	32.8	0	Ftw
WD 2307+548	LSPM J2309+5506E	DA	15.6	H	5531	0.65	4.16	16.4	0	B&L21
WD 2307−691	HD 218572B	DB	13.6	He	11086	0.57	0.48	21.1	0	Ftw
WD 2316−173	EGGR 264	DB	14.1	He	11533	0.64	0.51	25.5	0	Itw
WD 2326+049	V* ZZ Psc	DAZ	13.1	H	11528	0.63	0.46	17.5	0	B&L21
WD 2329+407	EGGR 160	DA	13.9	H	16664	0.61	0.14	35.7	0	S&S95, Itw
WD 2333−165	GD 1192	DA	13.4	H	13506	0.59	0.27	24.3	0	Ftw
WD 2336−079	GD 1212	DA	13.3	H	10872	0.61	0.52	18.7	0	B&L21
WD 2341+322	LAWD 93	DA	13.0	H	12586	0.61	0.35	18.6	0	B&L21

Key to the abbreviations used in col. 11: B&L21: original references are given in Table 1 of Bagnulo & Landstreet (2021). Etw: this work, using the ESPaDOnS instrument; Itw: this work, using the ISIS instrument; Ftw: this work, using the FORS instrument. Azn+04: Aznar Cuadrado et al. (2004); B&L18: Bagnulo & Landstreet (2018); Jor+07: Jordan et al. (2007), Kaw+07: Kawka et al. (2007); Koe+98: Koester et al. (1998) Lan+12: Landstreet et al. (2012); L&B19: Landstreet & Bagnulo (2019b); L&B20: Landstreet & Bagnulo (2020); Lie+77: Liebert et al. (1977); Lie+93: Liebert et al. (1993); S&S95: Schmidt & Smith (1995); Sch+92: Schmidt et al. (1992); Swe+94: Swedlund et al. (1974).

We note that star WD 0316−849 = RE J0317−853 = EUVE J0317−853 = V* CL Oct is often confused with star WD 0325−857 = EQ J0317-855 = LB 9802, a hot and young non magnetic WD with which it forms a physical VB system.